December 2009 Volume 5 Issue 4

Trade Science Inc.

Materials Science

An Indian Journal

Full Paper

MSAIJ, 5(4), 2009 [364-375]

Study on the mechanism of nucleation and development of porous nanostructure of anodic alumina films

G.Patermarakis

School of Chemical Engineering, Department of Materials Science and Engineering, National Technical University, Iroon Polytechniou 9, Zografou 157 80, Athens, (GREECE)

E-mail : gpaterma@central.ntua.gr

Received: 9th July, 2009 ; Accepted: 19th July, 2009

ABSTRACT

The growth of porous anodic alumina films in a single step anodising of Al in sulphuric and oxalic acid electrolytes was studied by chronopotentiometry and the surface of films and the imprint of films on Al metal surface in steady state were examined by SEM. It was shown that at the initiation of steady state the outer thin surface layer consists of nanocrystallites. On prolonged anodising due to chemical dissolution of a thin surface layer they disappear and enlarged pore mouths and a relatively compact interpore material are exhibited while the porous layer with the characteristic columnar cellular hexagonal structure constantly develops in the metal|oxide interface region. These predict that the actual reason for the nucleation of pores in the flat barrier layer and their development to pockets and then to channel-like pores in the preceding transient stages is related with a nanocrystalline recrystallization / transformation and densification of oxide towards the surface of rare oxide formed in the metal|oxide interface and the base surface of developed pockets or pores.

KEYWORDS

Anodic alumina;
Porous nanostructure;
Mechanism of nucleation and development.

INTRODUCTION

The porous anodic alumina films are formed by Al anodising most frequently in oxalic, chromic, phosphoric, sulphuric acid (and other sulphate) solutions and less frequently in malonic, tartaric, citric, etc, acid solutions. The pore forming anodising of Al is characterised, e.g. for oxalic, sulphuric and phosphoric acid electrolytes, by a transient stage, where a flat barrier layer is formed on the surface of which pores are later nucleated towards its end[1-5], followed by another transient stage where pores are developed and organized yielding the characteristic structure of these films[3-14] that is finally followed by the steady state stage. The embryo of the porous structure observed in steady state thus appears in the first transient stage[1-5] and is integrated in the second one. The steady state structure of films is characterized as a close-packed array of approximately hexagonal, columnar cells, each of which contains an elongated, roughly cylindrical, pore normal to the surface extending between the film's external surface and the Al_2O_3|Al interface, where it is sealed by a thin, compact, hemispherical shell shaped barrier type oxide layer with thickness roughly around 1 nm per V of applied voltage[15-17]. The structure of films is defined by the surface density of pores, usually of the order $10^9 - 10^{11}$

cm^{-2}, base diameter of pores, of the order of a few up to several tens nm, shape and ordering degree of pores, which depend on the kind of electrolyte and conditions of Al anodising[16-19]. The oxide, examined after anodising, is an almost anhydrous amorphous (or nanocrystalline) γ or γ'-Al_2O_3 material[16,17,20]. Protons and electrolyte anions are embodied in small amounts variable across the barrier layer and pore walls depending on electrolyte kind and conditions[4,16-18,20]. Anions exist in a pore surface layer leaving an anion almost free layer near the metal and cell boundaries[4,18].

Due to their peculiar nanometer scale porous structure, physicochemical properties and strong adherence to the Al surface, these films find numerous applications such as protection, decoration and upgrading of mechanical properties of Al, catalysis, rechargeable batteries, magnetic memories, nuclear reactors, fuels cells, as templates for synthesising emitters, in nanoscience-nanotechnology, etc[6,21-24]. Perfect hexagonal structure in surface domains of area comparable to 1 μm^2, if desired, can be achieved by two or more steps anodising after the selective removal of film, where however the basic structure, imprinted on the Al metal substrate, is established in the first and can be improved in next steps[23].

Despite the large amount of work done heretofore, most of which is cited in[23,24], a generally adopted integrated theory satisfactorily describing the origin of emergence of pores nuclei and their progress to completion as pores is still basically unknown. The nucleation and development of pores is usually attributed to a thermally and / or field assisted chemical dissolution of film surface which however fails to explain satisfactorily the experimental results of film growth. Recently[6,25,26] the ionic migration of O^{2-} and Al^{3+} across the barrier layer during the steady state growth of porous films was studied in $H_2C_2O_4$ and H_2SO_4 electrolytes. The formulated relevant electrochemical high field kinetic models predicted a variation of local oxide density across the barrier layer from ≈ 2.6 g cm^{-3} near the metal|oxide interface to higher enough values near the oxide|electrolyte interface. Along the lines of these studies, in this work the progress of structure of both the surface of film and of Al substrate surface during anodising in steady state was studied by SEM. The findings of this work predict that the origin of nucleation and development of pores and of the entire porous structure is the recrystallization and densification of oxide towards the surface of the rare oxide formed in the metal|oxide interface at the above density, rendering unnecessary the adoption of other assistive assumptions not adequately provable, to explain the mechanism of nucleation and development of porous structure.

EXPERIMENTAL

Al anodising was performed at current density (j) = 15 mA cm^{-2} and bath temperatures (T) = 25 and 35 ($\pm$ 0.1 – 0.2) ^oC in vigorously stirred solutions of the most usually used pore forming electrolytes H_2SO_4, at concentration (c_a) =1.5 M (15% w/v) often met in the literature (pH = 0.131 at 25 ^oC), and $H_2C_2O_4$ solution for comparison also at c_a = 1.5 M (pH = 0.442 at 25^oC) at anodising times (t) up to 40 min. The employed j is relatively low and the T's are middle compared with those usually employed, varying from ≈ 0 up to ≈ 60 ^oC[23], which assure that the necessary voltage for all t's is not high enough to avoid high rate of heat evolution in the anode that would notably rise the real anodising T in the anode, more with rising j and dropping T[19]. The employed middle c_a and T's however assure non negligible rate of chemical dissolution by the electrolyte of film surface e.g. after the formation of porous structure for reasons which will become legible later. It is noted that the $H_2C_2O_4$ solution was just saturated at 25 ^oC but it was clearly unsaturated at 35 ^oC. Two face Al sheets anodic electrodes 3×5 cm with thickness 0.3 mm and purity = 99.95% (Merck - proanalysi), with total geometric surface area to be anodised (S_g) = 50.45 cm^2, and two Pb cathodic electrodes of similar geometry were used.

Prior to anodising the Al specimens were chemically etched by chromophosphoric acid solution which removes the oxide on the metal surface (either natural or anodic) and leaves intact the metal[16,17,19,23], washed by distilled water and dried in an air stream. After anodising, carried out as described in detail elsewhere[19], the specimens were washed, neutralized to remove electrolyte probably remaining in narrow pores, washed and dried. Then, specimens were divided into two equal parts one of which would be used for the SEM examination of oxide surface. The other part was

etched to selectively remove the oxide formed on the Al surface during anodising and treated as above to examine the Al surface by SEM.

Al anodising was followed chronopotentiometrically. The anodic potential (e.g. vs. SHE) almost coincides with the potential drop from the metal|oxide (m|o) to the oxide|electrolyte (o|e) interface[27,28] and is close to the anodising voltage[27]. For ease the latter was recorded. Chronopotentiometric curves are used, among others, to define the boundaries of transient stages and the start time of steady state stage.

RESULTS AND DISCUSSION

The anodising voltage (ΔV) vs. t plots up to the maximum t employed appear in Figure 1a while Figure 1b presents a magnification of plots in the range of low t's. Figure 1 provides the following already noted successive stages: The stage 0B with abrupt initially almost linear rise of ΔV gradually declining with increasing rate towards its end. It corresponds to the transient stage of growth of the initial flat barrier layer in the last range of which, between roughly 2/3 of its duration (around 10 – 15 s in the employed electrolytes and conditions) and its end, the porous structure is nucleated[1-5], i.e. in the region AB. The duration of stage 0B decreases with T and is higher for $H_2C_2O_4$ solution. The final maximum ΔV value strongly rises with decreasing T and is much higher for $H_2C_2O_4$. The stage BC of the subsequent drop of ΔV within a t of the order of 1 min, longer for $H_2C_2O_4$, in which the pore / cell system units develop and cover gradually all the surface and are self-organised to a more regular ordering within domains comparable e.g. to metal grain surfaces towards the Al substrate side[6-14], the proper almost final number of cells / pores is set up and a steady state pore base diameter, nature / composition of barrier layer and electrolyte composition in pores is finally achieved. The duration of this stage also faintly drops with T and is shorter for H_2SO_4 electrolyte while the dependence of the final ΔV on conditions is similar to that of the previous maximum ΔV. The stage CD, which represents the steady state stage, where ΔV remains constant or changes slightly. Similarly as above ΔV increases with decreasing T and is much higher for $H_2C_2O_4$. The final cellular columnar porous structure has been already established in the start of this stage[6].

The commonly accepted geometric representation

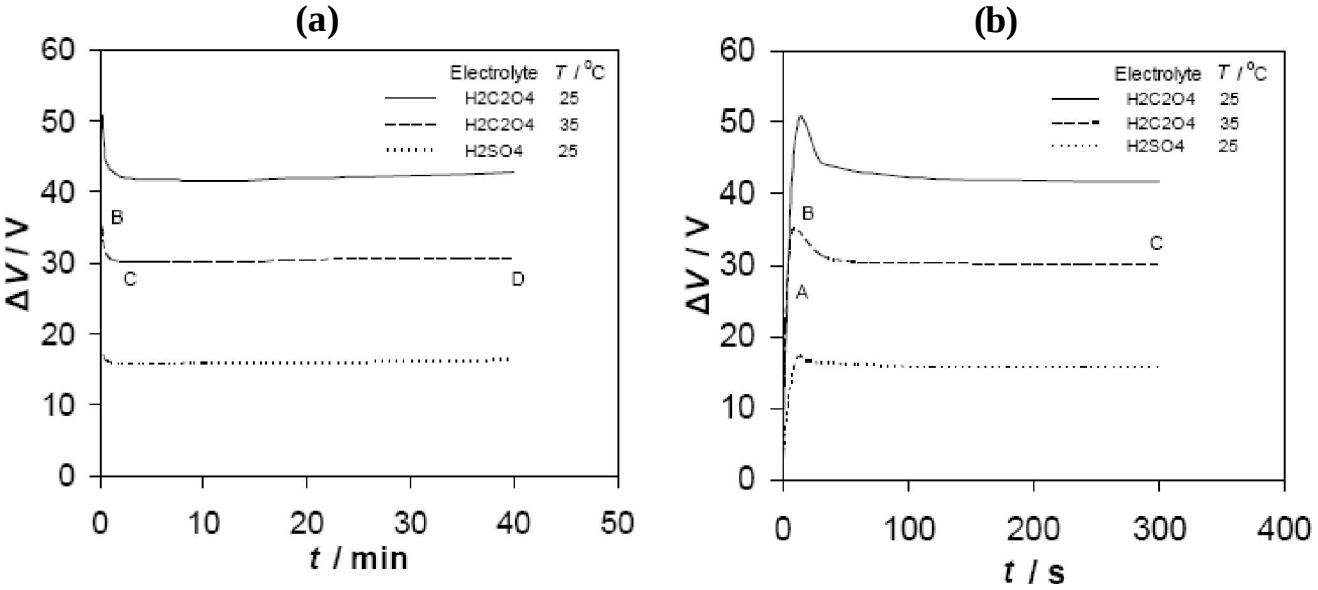

Figure 1 : (a) Plots of ΔV vs. t during Al anodising in oxalic and sulphuric acid solutions at c_a = 1.5 M, j = 15 mA cm^{-2} and T = 25 and 35 °C up to the higher t's employed. (b) Magnification of plots in the region of low t's.

of development of porous structure in relation to the ΔV vs. t plots[1-5,23,24] is given in Figure 2 where a, b, (c, d) and e correspond respectively to the substage 0A of flat film growth, substage AB of pore nucleation, stage

BC of pockets development and their transformation to channel-like pores and stage CD of steady state growth of the permanent porous structure.

The potential drop in the anode from Al to electro-

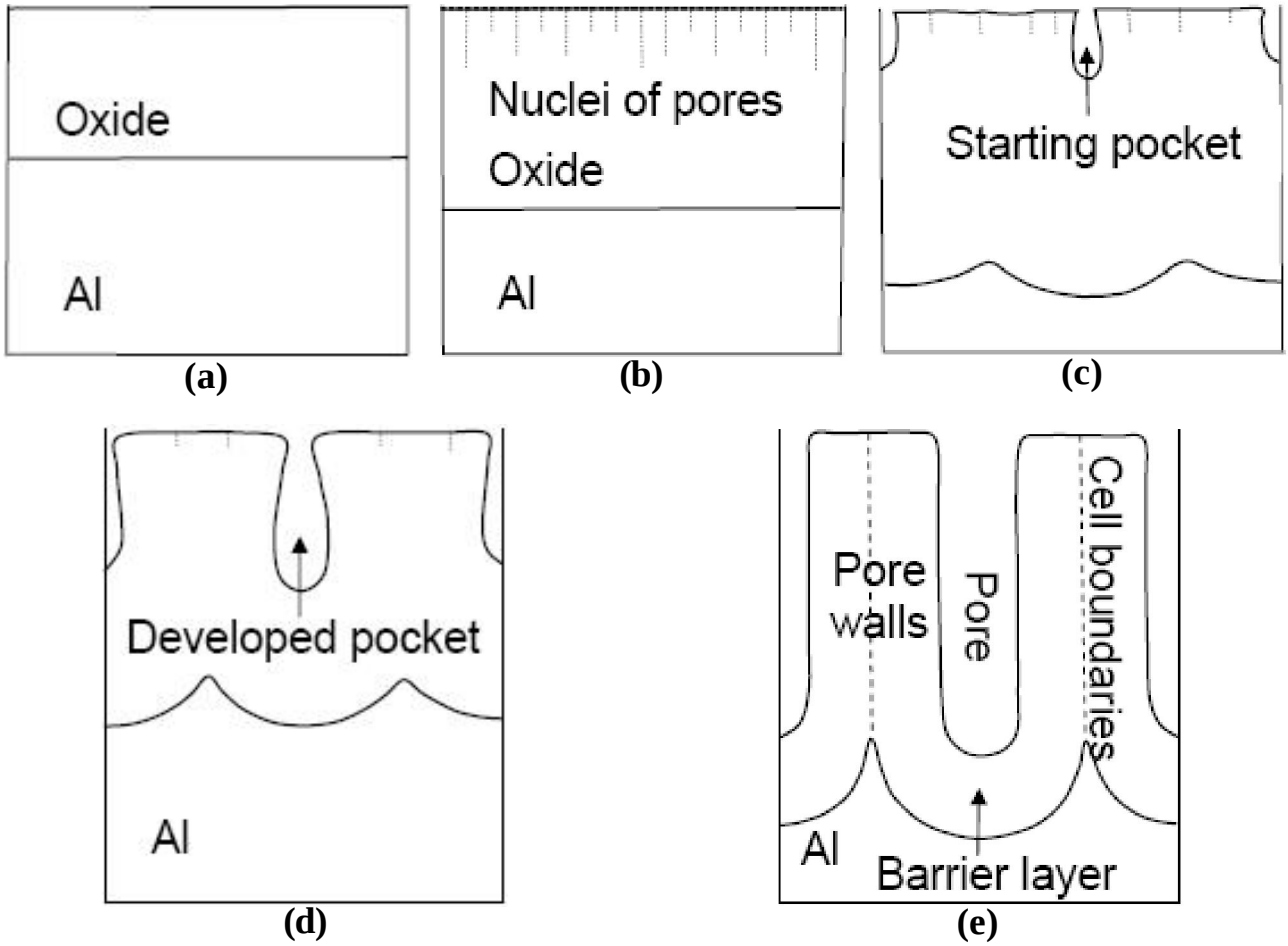

Figure 2 : Schematic cross film sectional representation of the generally adopted geometric mechanism of the appearance of pores nuclei, their transformation to pockets and then to pores and of the development of characteristic porous structure during the three different stages of Al anodising[1-5,23,24]: (a) Flat barrier layer prior to pores nucleation during the first substage of the first transient stage, 0A in Figure 1. (b) Nucleation of pores during the seconbd substage of the first transient stage, AB in Figure 1. (c,d) Transformation of pores nuclei to pockets and then to pores during the second transient stage, BC in Figure 1. (e) Growth of porous structure of anodic film in steady state, CD in Figure 1, where the characteristic nanostructural features, such as the channel-like pores, scalloped barrier layer, pore walls, cell boundaries and metal|oxide interface, are shown.

lyte ($\approx \Delta V$) and the occurring processes are divided into those in the barrier layer oxide and in the m|o and o|e interfaces. For sufficiently thick flat barrier layer grown during the stage 0B, e.g. that grown for $t \geq 1$ s at the j employed, or for the scalloped one in stages BC and CD the potential drops in interfaces are tiny compared to that in the oxide[28,29]. Thus the change of ΔV with t, T and j reflects the effect of the thickness and nature / composition / structure of barrier layer, that are in turn affected also by t, T, j and electrolyte composition, and the effect of T and j per se on ΔV defined by kinetic models[25,26]. The higher ΔV for lower T and for $H_2C_2O_4$ than for H_2SO_4 at the characteristic t's like t_A, t_B and t_C are due primarily to the corresponding thicker barrier layer either flat or scalloped and secondarily to other electrochemical kinetic parameters[25,26].

During the growth of porous films oxide is formed exclusively in the m|o interface where the real rate of oxide production is given by $kS_g j t_{an}$ [6,25,26], where t_{an} is the transport number of O^{2-} anions migrating in the ad-

jacent oxide bulk (while that of Al^{3+} cations is $t_{ca} = 1 - t_{an}$). By the method outlined elsewhere[6] the transport number t_{an} was found 0.742 and 0.683 for oxalic acid at $T = 25$ and 35 °C and 0.729 for sulphuric acid at $T = 25$ °C respectively. In steady state t_{an} drops with T (and rises with j[6,25,26]) while it is almost independent of electrolyte kind and composition. Because t_{an} increases with the apparent j (and thus with the real j (j_t) in the m|o interface where $j_t = j/2.093$[28]) it is expected to decrease slightly from the first transient substage 0A or stage 0B to the steady state stage CD, Figure 1, and thus the real rate of oxide production also slightly drops.

In Figure 3 SEM micrographs are shown of the surface of films grown in $H_2C_2O_4$ at $T = 25$ °C (a-c) and 35 °C (d) at $t = 5$ min ($\approx t_C$) (a,d), 10 min (b) and 40 min (c). Embossed nanocrystalline surfaces appear. In Figure 3a, b, d pores are hardly discerned due to their narrowness. But at $t >> t_C$ pores become easily discerned, Figure 3c, due to chemical dissolution by the electrolyte of a thin surface oxide layer and of their mouths and thus to pore widening on film surface. The pores seem to appear in arbitrarily non-ordered surface sites, Figure 3c. On increasing t the features of the embossed surface are initially reinforced and then they

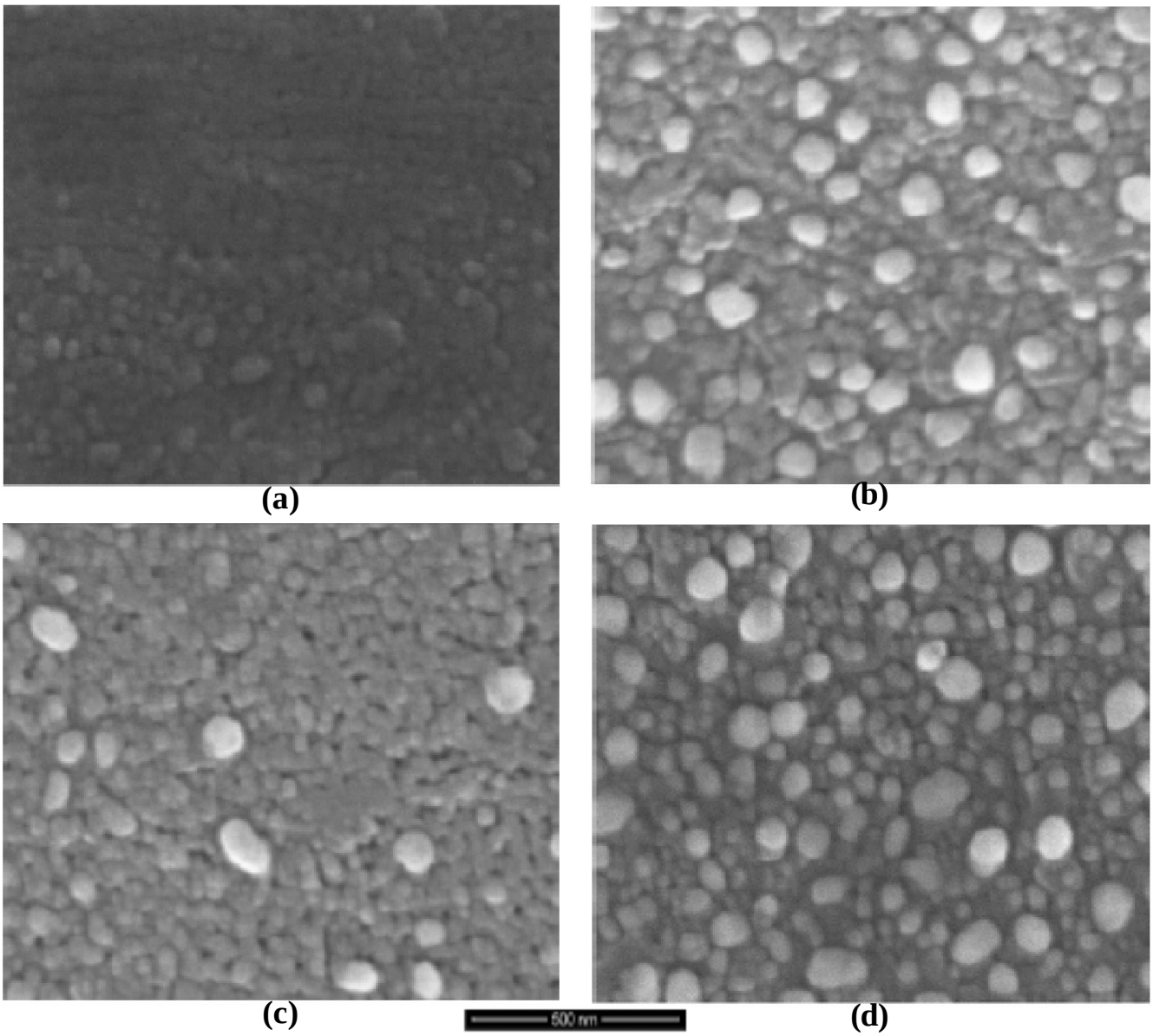

Figure 3 : SEM micrographs of the surface of films prepared in oxalic acid at $c_a = 1.5$ M, $j = 15$ mA cm^{-2}, $T = 25$ °C (a-c) and 35 °C (d) and $t = 5$ min (a,d), 10 min (b) and 40 min (c).

gradually decay mainly at higher *t*'s, Figure 3a-c. Comparison of Figures 3a-c (a,b at $T = 25^{o}C$ - saturated bath and c at $T = 35^{o}C$ - unsaturated bath) proves that the nanocrystalline surface aspect cannot be attributed to any effect of saturated bath.

In Figure 4 SEM micrographs are shown of the surface of films grown in H_2SO_4 at $T = 25\ ^{o}C$ and $t = 5$ min ($\approx t_C$) (a), 10 min (b) and 40 min (c). Embossed nanocrystalline surface also appears and pores are also hardly discerned at $t \approx t_C$, Figure 4a, but at $t = 10$ min and mainly at $t = 40$ min ($>> t_C$) the pores become easily discerned, more than in $H_2C_2O_4$ films at comparable *t* due to the much stronger ability of H_2SO_4 than that of $H_2C_2O_4$ for chemical dissolution of oxide[30] which is also predicted from the lower pH and thus higher H_3O^+ activity for H_2SO_4 electrolyte. The pore surface density of H_2SO_4 films is also higher than that of $H_2C_2O_4$ films. Simultaneously the features of nanocrystalline embossed surface seem to be reinforced up to *t* around t_c and then they gradually decay, but have not however completely disappeared even at $t = 40$ min, and the interpore surface material becomes smoother and more compact.

Within the steady state stage the size of

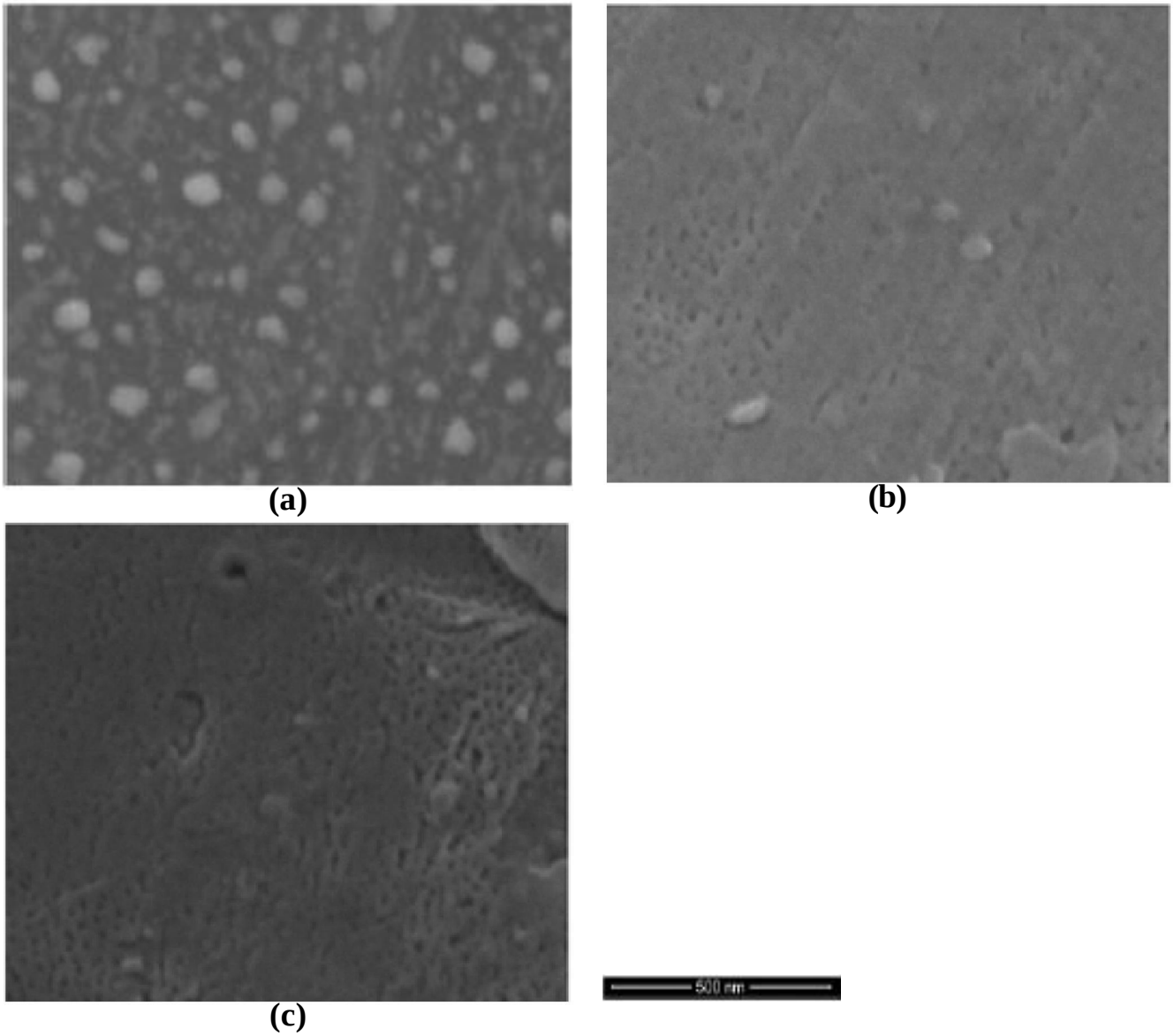

Figure 4 : SEM micrographs of the surface of films prepared in sulphuric acid at $c_a = 1.5$ M, $j = 15$ mA cm^{-2}, $T = 25\ ^{o}C$ and $t =$ 5 min (a), 10 min (b) and 40 min (c).

nanocrystallites is reduced due to chemical dissolution of oxide by the electrolyte while some of them may be also detached dropping to solution where the supporting them underlying rarer material is dissolved as expected easier than nanocrystallites. Considering a rate of film chemical dissolution reaction by the H_2SO_4 electrolyte of the order of ≈ 0.1 nm min^{-1}[19] and the time of 40 min where the largest nanocrystallites on surface seem to have not completely vanished, the larger size of these crystallites seems to be > 4 nm, as indeed observed in Figures 3 and 4. The rate of film thickness (h) increase in steady state is given by $dh/dt = zjt_{an}$ where $z \approx 6.982\times10^{-1}$ cm^3 C^{-1} ($H_2C_2O_4$ electrolyte[25]) and $z \approx 6.983\times10^{-1}$ cm^3 C^{-1} (H_2SO_4 electrolyte[26]) and h at t = 40 min is thus ≈ 18.35 μm. Therefore in any case the thickness of surface layer of oxide dissolved by the electrolyte is negligible compared to the thickness of film grown at the same time interval. The non-uniform aspect of Figure 4c is evidently due to the variable / distributed nanocrystallite sizes in a thin layer of the initial film surface and thickness of surface layer dissolved by electrolyte, the rate of which dissolution may be affected by any nm scale surface roughness, local stirring conditions, related topoelectrochemical parameters and flaws of initial Al surface. More uniform aspect is however expected at $t >> 40$ min as the surface layer oxide is further dissolved[19].

The maximum possible organization of cells / pores in deeper oxide layers permitted by parameters of anodising process, like ΔV in steady state etc[23], is already established at $t \approx t_C$ and it continues to be steadily reproduced for $t > t_C$, as it is revealed by the SEM micrographs of the imprints of scalloped barrier layer on Al metal, Figure 5. The ordering of cells / pores in Figure 5c deviates noticeably from a perfect hexagonal as the steady state ΔV is ≈ 30 V, markedly differing from $\Delta V \approx 45$ V of optimum hexagonal ordering for oxalic acid films[23]. But in Figure 5a, b where ΔV was ≈ 42 - 43 V, close to 45 V, the ordering approaches perfect hexagonal in finite surface domains. Bright entities are sites of ordering violation where protrusions of Al metal appear, while the large bright entity in Figure 5c is most probably due to surface impurity (foreign particle). The cell width (D_c) is ≈ 115.9 and 83.5 nm and the pore surface density (n) is $\approx 9.92\times10^9$ and 1.91×10^{10} cm^{-2} ($nD_c^2 = 4/3$[28]) at T = 25 and 35°C. Their variation with T agrees with literature data[16,17,23,31]. The same trends of D_c and n variations are also valid with decreasing j and increasing c_a[23]. Similar behaviour was observed also for the H_2SO_4 films as regards the change of the Al surface structure with t in steady state where however the surface density of pores / cells is larger than in $H_2C_2O_4$ films, $n \approx 1.3\times10^{11}$ cm^{-2} and $D_c \approx 32$ nm, while their ordering is strongly violated due to that ΔV in steady state, ≈ 16 V, deviates strongly from the maximum ordering $\Delta V \approx 25$ V[23]. Citation of relevant micrographs was judged unnecessary since they do not offer any additional utilizable information. The constant ΔV during the steady state CD implies that the D_c, pore base diameter and thickness of barrier layer remain constant.

The above behaviour revealed by SEM is explained as follows:

The oxide is formed in the m|o interface in steady state CD (and as expected in transient stages 0B and BC) that is an almost pure rare oxide material with density 2.60 g cm^{-3} for $H_2C_2O_4$[25] and 2.52 (≈ 2.6) g cm^{-3} for H_2SO_4[26] films. This oxide must have a bcc lattice regarding the Al^{3+} sublattice, with lattice parameter 0.402 nm essentially coinciding with the fcc lattice parameter of Al, 0.4041 nm. This is an unstable lattice, existing only under the high strength field (of the order of 10^7 V cm^{-1}[27]) action, which must be transiently stabilized around and beyond the m|o interface by electroexpansion stresses created as expected by a stoichiometric excess of Al^{3+} in the oxide bulk. These stresses are counterbalanced by electroresticting stresses between the positively charged oxide and negatively charged double layer in the o|e interface[32,33].

The oxide formed in the m|o interface is ≈ 37% rarer than γ-Al_2O_3 with density ≈ 4 g cm^{-3}[34] that is the most related form of oxide with that of anodic oxide obtained after anodising and oxide relaxation[16,17,20]. The γ-Al_2O_3 is considered a defect spinel structure (space group $Fd\bar{3}m$)[35] with O^{2-} in 32e Wyckoff positions which can be viewed approximately a 2×2×2 array of fcc unit cells[36]. It is characterized by vacancies in tetrahedral[37] or octahedral[38] sites rather randomly distributed from which tetrahedral sites empty in ideal spinel may be partially occupied in defect alumina structures[36,39]. The lattice parameter of γ-Al_2O_3 is 0.79 nm

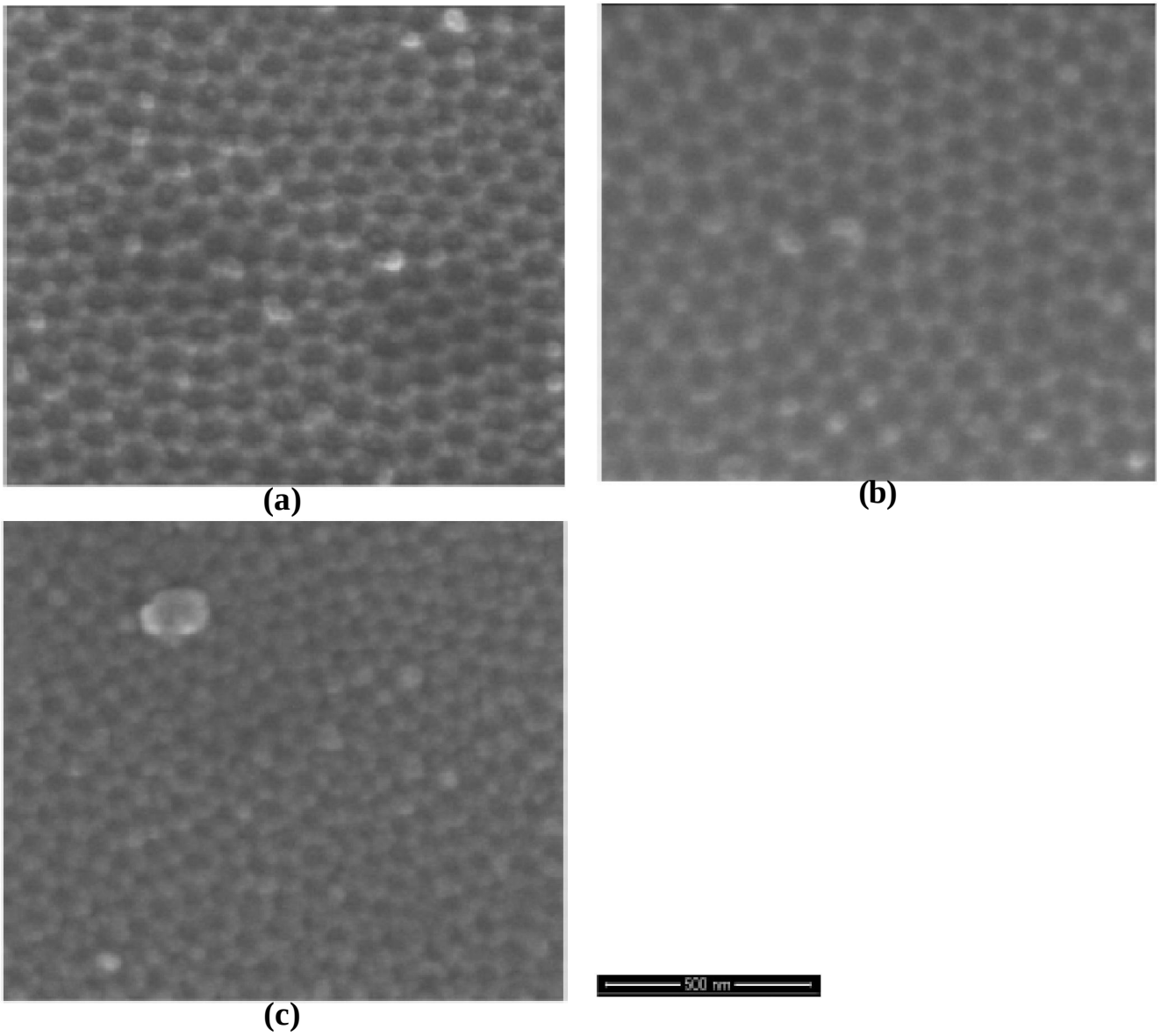

Figure 5 : SEM micrographs of the surface of Al after the selective removal of the oxide prepared in oxalic acid at c_a = 1.5 M, j = 15 mA cm^{-2}, T = 25 °C (a,b) and 35 °C (c) and t = 5 min (a,c) and 40 min (b) where the close packed hemispherical imprints of scalloped barrier layer units on Al surface are shown.

≈ 2×0.4060 nm. For nanocrystalline or amorphous oxide the relevant parameter will be on average slightly enlarged. Hence, a 2×2×2 array of bcc unit cells of transient lattice is convenient to be transformed to a cell of denser amorphous γ-Al_2O_3 oxide and on heating to crystalline γ-Al_2O_3 [40]. But the γ-Al_2O_3 lattice cell incorporates more suitably entered and arranged atoms than the 2×2×2 array of bcc unit cells of transient lattice, as demanded by its 37% higher density.

When the oxide formed in the m|o interface advances to the o|e interface, thus becoming less influenced by the lattice of Al metal, there is a spontaneous tendency for its unstable lattice to be transformed to the denser and more stable γ-Al_2O_3 [16,17,20] more towards the o|e interface in the form of nanocrystallites. Prior to t_A a continuous formation of unstable nuclei of nanocrystallites supposedly occurs which are soon deformed, probably affected by the high strength field in the region of m|o interface and up to some distance from it or, in other words, up to the surface of film formed up to $t \approx t_A$. The first position of integrated lattice transformation to nanocrystallites with structure resembling

that of γ-Al_2O_3 is thus a thin surface layer of oxide produced at $t = t_A$. At $t \approx t_A$ the first integrated stable nanocrystallites of denser and stable γ-Al_2O_3 are formed at arbitrary sites in the surface layer and their presence and development are fast spread in the whole surface, like an avalanche phenomenon, from A to B. These are rather neutral particles or anyway with lower Al^{3+} charge excess. Between nanocrystallites the oxide must have higher Al^{3+} excess and thus it may become rarer even than the initially formed oxide. The thin surface oxide layer is then prone to be ruptured in the regions of rarer material among nanocrystallites forming nuclei of pores. The formation of surface nanocrystallites, acting as a matrix, must also catalyze and propagate recrystallization to interior oxide layers.

The nuclei of pores appearing during the substage AB are transformed to pockets and then to pores in BC, Figures 1 and 2. Well beyond B and up to C the only process occurring in the hollowed film surface, which is now unaffected by the field, is the chemical dissolution reaction. Its rate is negligible compared with the rate of film mass and thickness growth[19,30]. The chosen electrolytes, c_a and T's assure relatively enhanced surface oxide dissolution by the electrolyte, as expected more for the remaining rare unruptured oxide among nanocrystallites rather than for nanocrystallites, capable of accentuating nanocrystallites within reasonable t, e.g. at $t \approx t_C$. Then, the film surface at $t > t_C$ must present a nanocrystalline embossed aspect, as indeed observed in Figures 3 and 4. From t_A or t_B up to t_C and beyond t_C the employed c_a and T's are able to bare and accentuate nanocrystallites but are unable to reduce fast their size. The features of the embossed nanocrystalline surface are thus initially reinforced, reaching their maximum intensity much earlier for H_2SO_4 than for $H_2C_2O_4$ films due to the higher dissolving ability of H_2SO_4 than that of $H_2C_2O_4$[30], and then they gradually decay on further dissolution of the surface oxide layer. On prolonged anodising however these surface nanocrystallites are finally dissolved and / or detached and the interpore material of hollowed surface layer becomes smoother, as in Figure 4c concerning H_2SO_4 films. From Figure 3a-c it is evident that such a situation will be attained for $H_2C_2O_4$ films at $t >> 40$ min. During the stage BC the continuing recrystallisation and concomitant shrinkage of oxide below the film external surface and towards the surface of nuclei units transformed to pockets which are then transformed to pores (transformation nuclei $\rightarrow$ pockets $\rightarrow$ pores) more towards their bases for $t > t_B$ reduces the thickness of pore walls widening the pockets or pores to the Al side, Figure 2c,d. The oxide becomes nanocrystalline / amorhous[20] but compact enough towards the base surface of pockets or pores. It is noted that the widening of pockets during their transformation to pores is also favoured by the slightly falling t_{an} and thus falling rate of oxide formation in the m|o interface.

In the second transient stage BC the nuclei of pores widen and lengthen with t and in this way these are transformed to pockets and then to channel-like pores, Figure 2c,d. As new oxide is formed in the m|o interface and is promoted to the bottom of nuclei $\rightarrow$ pockets $\rightarrow$ pores, the locale of electrochemical processes is shifted from film surface in substage 0B towards their surface, more to their depth. The recrystallisation, continuing also in this stage, is relocated occurring thus in the surface of nuclei $\rightarrow$ pockets $\rightarrow$ pores, more to their depth on increasing t. It is propagated to interior oxide layers, thus developing a gradient of shrinkage degree and of local oxide density (d_c) across the scalloped barrier layer. A stable distribution of d_c rising to the o|e interface with the largest achieved span determined by conditions is expected to be established across the barrier layer in steady state. This was indeed earlier shown by an entirely different (electrochemical kinetic[25]) method where it was found that in steady state the following equation interrelating kinetic, physical and nanostructural parameters

$$\mathbf{d_{c,a}(1 - 4^{-1}\pi n D_b^2) = d_{c,m|o} = d_{c,m|o} t_{an}^{-1} - d_{c,o|e} 4^{-1}\pi n D_b^2} \quad (1)$$

is valid, where $d_{c,m|o}$, $d_{c,o|e}$ and $d_{c,a}$ are the local density of oxide near the m|o and o|e interfaces and the average density across the barrier layer and D_b is the pore base diameter, from which it is inferred that

$$\mathbf{d_{c,o|e}^{-1} = t_{an}(1 - t_{an})^{-1}(d_{c,m|o}^{-1} - d_{c,a}^{-1})}. \quad (2)$$

The latter equation shows that $d_{c,o|e} > d_{c,a} > d_{c,m|o}$ or d_c actually rises from $d_{c,m|o} \approx 2.6$ g cm^{-3} at the m|o interface towards the o|e interface while $d_{c,a}$ lies in the region 3.21 - 3.52 g cm^{-3} depending on conditions[25]. It is noted that the D_b of films prepared here cannot be accurately determined by the above equations since the

precise values of $d_{c,a}$ or $d_{c,o|e}$ are unknown. All parameters $d_{c,a}$, $d_{c,o|e}$ and D_b together can be determined by a complex method[25], the citation of which is however beyond the study scope.

The ordering of cells / pores in BC towards the Al side must be due to the electroexpansion of positively charged anode, Al and oxide, developing repulsive stresses between Al and the gradually formulated units of scalloped barrier layer and pore walls around pore bases and between adjacent units, like densely packed touching, spherical, easily sliding objects with some elasticity, such as blown up balloons or bubbles on a surface. These are forced to become as possible arranged in each finite surface domain, like grain surface, according to the interrelated conditions: (i) tendency for occupancy of maximum possible area that is counterbalanced by a similar tendency of neighbouring units, (ii) highest surface 2D symmetry (that is hexagonal) best accommodating counterbalance of stresses between units to each surface direction, (iii) highest 3D shell symmetry (hemispherical), best accommodating counterbalance of electroexpansion (probably variable across the barrier layer related with the variable d_c) and electrorestriction stresses for each radial direction and at each barrier layer unit.

The spontaneous recrystallization and densification of oxide to the pore base surface together with the tendency of material to be organised under the above conditions (i) – (iii) are responsible for the uninterrupted continuous development of columnar, cellular, channel-like porous structure during the steady state when the conditions and composition of filling solution in the pore base region remain relatively unaltered.

As shown previously[6,25,26], the mechanism of film growth embraces: (i_1) Ejection and solvation of Al^{3+} at film surface of flat barrier layer type oxide during the first transient stage and at the surface of nuclei → pockets → pores more towards their base surface as t increases during the second transient stage and only at pore bases in steady state. (ii_1) Countermigration of O^{2-} surrounding Al^{3+} together with the rest required O^{2-} coming from the decomposition of H_2O after its dissociative adsorption. Thus the surface oxide is actually deformed to solvated Al^{3+} and migrating O^{2-}. This mechanism is consistent with the present results suggesting that the nucleation and development of porous structure is associated with a recrystallization process. Both support that electrochemical dissolution of oxide actually does not occur and is not involved in the nucleation and development of porous structure. The latter also does not demand the involvement of chemical dissolution of oxide by the electrolyte. This is indirectly intruded via the ability of electrolyte to solvate ejected Al^{3+} which is seemingly taken for oxide dissolution since Al^{3+} ejection apparently does not occur when oxide is not chemically dissolved in solution. Hence, the occurring oxide dissolution is of chemical only nature of negligible rate, compared with the rate of oxide mass production and the rate of thickness growth of the whole film and its porous layer, which is not involved in the development of porous structure. The theory formulated here is thus self-contained and consistent, not requiring the adoption of other processes like thermally or field assisted dissolution of oxide for the formation of nuclei, pockets and pores. It can thus justify the growth of films in very low T's, even < 0 °C[23] when certainly electrolyte is still in liquid state, where the rate of chemical dissolution is practically zero. It is noted that to fully develop the cited theory further work is necessary aiming at the elucidation of the mechanisms by which the recrystallization of rare oxide produced in the m|o interface is put forward and completed during the transient stages 0B and BC as well as of the continuous recrystallization and densification of oxide across the barrier layer during the steady state stage from the m|o to the o|e interface.

CONCLUSIONS

1. Results for films grown in the most commonly employed pore forming electrolytes, oxalic and sulphuric acid solutions, during a single step Al anodising showed that the surface of oxide at the initiation of steady state consists of nanocrystallites. On prolonged anodising they gradually disappear as a result of film surface dissolution by the electrolyte exhibiting enlarged pores mouths and a rather compact interpore surface material. At the same time the porous layer and its characteristic structure constantly grow in the region of barrier layer between Al and porous layer.
2. These results predict that the origin of pores nucle-

ation in the first transient stage is the spontaneous recrystallization of the rare oxide lattice formed in the m|o interface, accommodated with the Al lattice, to nanocrystallites of denser oxide in the surface of flat film towards the end of this stage. The rarer oxide between nanocrystallites is prone to be ruptured, assisted by rejection and fast solvation of Al^{3+} and countermigration of adjacent O^{2-}, anticipated by the mechanism of film growth, and by penetration of electrolyte anions in formed voids all of which coworking yield crack-like holes, the nuclei of pores.

3. The origin of nuclei transformation initially to pockets and then to channel-like pores is the gradual shift of location of charge exchange processes from the film surface to the bottom of nuclei → pockets → pores together with the continuous formation of rare oxide in the m|o interface with constant d_c and the enhanced recrystallization and densification of oxide from the m|o to the o|e interface yielding the scalloped barrier layer. A transient d_c distribution is established across the barrier layer stabilised at the end of the second transient stage.
4. This is a self-contained theory not requiring the adoption of other non-provable suggestions to explain the mechanism of growth of porous structure. It is expected to assist the elucidation of the effect of anodising conditions on the recrystallization processes and on the resulting porous structure, to assist the explanation of the existence of best conditions for optimum structure ordering and to contribute to structure design with evident significance for the numerous applications of porous anodic alumina films.

REFERENCES

[1] V.F.Surganov, G.G.Gorokh; Mater.Lett., **17**, 121 **(1993)**.
[2] V.Surganov, C.Janson, J.C.G.Nielsen, P.Morgen, G.Gorokh, A.N.Larsen; Electrochim.Acta, **33**, 517 **(1988)**.
[3] C.J.Dell'Oca, P.J.Fleming; J.Electrochem.Soc., **123**, 1487 **(1976)**.
[4] V.P.Parkhutik; Corros.Sci., **26**, 295 **(1986)**.
[5] V.P.Parkhutik, V.I.Shershulsky; J.Phys.D.Appl., **25**, 1258 **(1992)**.
[6] G.Patermarakis, J.Chandrinos, K.Masavetas; J.Solid State Electrochem., **11**, 1191 **(2007)**.
[7] O.Jessensky, F.Müller, U.Gösele; Appl.Phys.Lett., **72(10)**, 1173 **(1998)**.
[8] L.Zhang, H.S.Cho, F.Li, R.M.Metzger, W.D.Doyle; J.Mater.Sci.Lett., **17**, 291 **(1998)**.
[9] O.Jessensky, F.Müller, U.Gösele; J.Electrochem. Soc., **145**, 3735 **(1998)**.
[10] K.Nielsch, J.Choi, K.Schwirn, R.B.Wehrspohn, U.Gösele; Nano Letters, **2(7)**, 677 **(2002)**.
[11] A.P.Li, F.Müller, A.Birner, K.Nielsch, U.Gösele; J.Appl.Phys., **84(11)**, 6023 **(1997)**.
[12] A.P.Li, F.Müller, U.Gösele; Electrochem.Solid State Lett., **3(3)**, 131 **(2000)**.
[13] H.Masuda, M.Yotsuya, M.Asano, K.Nishio, M.Nakao, A.Yokoo, T.Tamamura; Appl.Phys.Lett., **78(6)**, 826 **(2001)**.
[14] H.Pan, J.Lin, Y.Feng, H.Gao; IEEE Transac. Nanotechnol., **3**, 462 **(2005)**.
[15] F.Keller, M.S.Hunter, D.L.Robinson; J.Electrochem. Soc., **100**, 411 **(1953)**.
[16] J.W.Diggle, T.C.Downie, C.W.Goulding; Chem.Rev., **69**, 365 **(1969)**.
[17] L.Young; 'Anodic Oxide Films', Academic Press, London, **(1961)**.
[18] G.E.Thompson, R.C.Furneaux, G.C.Wood; Corros.Sci., **18**, 481 **(1978)**.
[19] G.Patermarakis, P.Lenas, Ch.Karavassilis, G.Papayiannis; Electrochim.Acta, **36**, 709 **(1991)**.
[20] G.Patermarakis, P.Kerassovitou; Electrochim.Acta, **37**, 125 **(1992)**.
[21] C.R.Martin; Chem.Mater., **8**, 1739 **(1996)**.
[22] N.Kovtyukhova, T.E.Mallouk; Adv.Mater., **17**, 187 **(2005)**.
[23] G.D.Sulka; 'Highly Ordered Anodic Porous Alumina Formation by Self-Organized Anodizing', in A.Eftekhari Ed., Nanostructured Materials in Electrochemistry, Wiley-VGH, Wienheim, 1-116 **(2008)**.
[24] P.G.Sheasby, R.Pinner; 'The Surface Treatment and Finishing of Aluminium and Its Alloys', 6th Ed., ASM International & Finishing Publications Ltd, USA-UK, **(2001)**.
[25] G.Patermarakis, Ch.Karayianni, K.Massavetas, J.Chandrinos; J.Solid State Electrochem., in press, first electronic publication.
[26] G.Patermarakis, K.Moussoutzanis; Electrochim. Acta, **54**, 2434 **(2009)**.
[27] G.Patermarakis, K.Moussoutzanis, J.Chandrinos; J.Solid State Electrochem., **6**, 39 **(2001)**.

[28] G.Patermarakis, K.Moussoutzanis; Electrochim. Acta, **40**, 699 **(1995)**.
[29] J.E.Houser, K.R.Heber; J.Electrochem.Soc., **153**, B566 **(2006)**.
[30] Patermarakis, K.Masavetas; J.Electroanal.Chem., **588**, 179 **(2006)**.
[31] Y.C.Sui, B.Z.Cui, L.Martínez, R.Perez, D.J.Sellmyer; Thin Solid Films, **406**, 64 **(2002)**.
[32] G.E.Thompson, Y.Xu, P.Skeldon, K.Shimizu, S.H.Han, G.C.Wood; Phil.Mag., **B55**, 651 **(1978)**.
[33] S.J.Garcia-Vergara, P.Skeldon, G.E.Thompson, H.Habazaki; Electrochim.Acta, **52**, 681 **(2005)**.
[34] R.C.Weast Ed.; 'Handbook of Chemistry and Physics', 60th Ed., CRC Press, Boca Raton, B-52 **(1980)**.
[35] B.C.Lippens, J.H.De Boer; Acta Crystallogr., **17**, 1323 **(1964)**.
[36] T.Hahn; 'International Tables of Crystallography', Luwer Academic Publishers, London, **A**, **(1995)**.
[37] S.D.Mo, Y.N.Xu, W.Y.Ching; J.Amer.Cer.Soc., **80**, 1193 **(1997)**.
[38] J.M.McHale, A.Navrotsky, A.J.Perrota; J.Phys.Chem., **101**, 603 **(1997)**.
[39] R.S.Zhou, R.L.Snyder; Acta Crystallogr., **B47**, 617 **(1991)**.
[40] E.Ruckenstein, Y.F.Chu; J.Catal., **52**, 109 **(1979)**.